Available online at www.sciencedirect.com
SCIENCE DIRECT®
C. R. Physique 6 (2005) 864–875
COMPTES RENDUS PHYSIQUE
http://france.elsevier.com/direct/COMREN/

Spectroscopy and planetary atmospheres/Spectroscopie et atmosphères planétaires

Atmospheric and meteorological Lidar: from pioneers to space applications

Pierre H. Flamant

Institut Pierre Simon Laplace, laboratoire de météorologie dynamique, École polytechnique, 91128 Palaiseau cedex, France

In memoriam Gérard Mégie

Abstract

The 'Light Detection and Ranging' technique, or Lidar, is a laser application to remote sensing. Lidar was in the laboratory stage in the 1960s and in less than 40 years it became a serious candidate for space applications at the turn of the 21st century. Over the years, the Lidar community made significant contributions to Lidar sciences and advancing the technique that makes Lidar an inevitable partner in geophysics and Earth observation. The French community, especially the Service d'Aéronomie and Laboratoire de Météorologie Dynamique, have been involved since the beginning in the Lidar venture and made significant contribution. ***To cite this article: P.H. Flamant, C. R. Physique 6 (2005).***

Résumé

Les Lidars atmosphériques et météorologiques : des pionniers au spatial. La technique Lidar est une application du laser à la télédétection. Le Lidar qui en était au stade du développement de laboratoire dans les années 1960, est devenu en moins de 40 ans un candidat sérieux pour les applications spatiales en ce début de 21e siècle. Au fil du temps, la communauté Lidar a contribué de manière significative aux activités scientifiques et aux avancées techniques qui font du Lidar un acteur incontournable en géophysique et en Observation de la terre. La communauté française, et tout spécialement le Service d'Aéronomie et le Laboratoire de Météorologie Dynamique, s'est impliquée dès le début dans l'aventure Lidar et a pu ainsi apporter sa contribution a l'ensemble. ***Pour citer cet article : P.H. Flamant, C. R. Physique 6 (2005).***

Keywords: External geophysics; Active remote sensing; Lidar; Laser system

Mots-clés : Géophysique externe ; Télédétection active optique ; Lidar ; Instrumentation laser

1. Introduction

The 'Light detection and Ranging' technique, or Lidar, is a laser application to remote sensing that operates day and night, contrary to passive remote sensors that rely on solar light. In the infrared Lidar offers much better vertical resolution due to poor thermal contrast between lower atmosphere and the underlying surface. Lidar was in the laboratory stage in the 1960s when the first laser was demonstrated. In less than 40 years it became a serious candidate for space applications at the turn of the 21st century. The geophysical applications cover short and long ranges up to hundreds of kilometers either from the

E-mail address: flamant@lmd.polytechnique.fr (P.H. Flamant).

1631-0705/$ – see front matter
doi:10.1016/j.crhy.2005.09.006

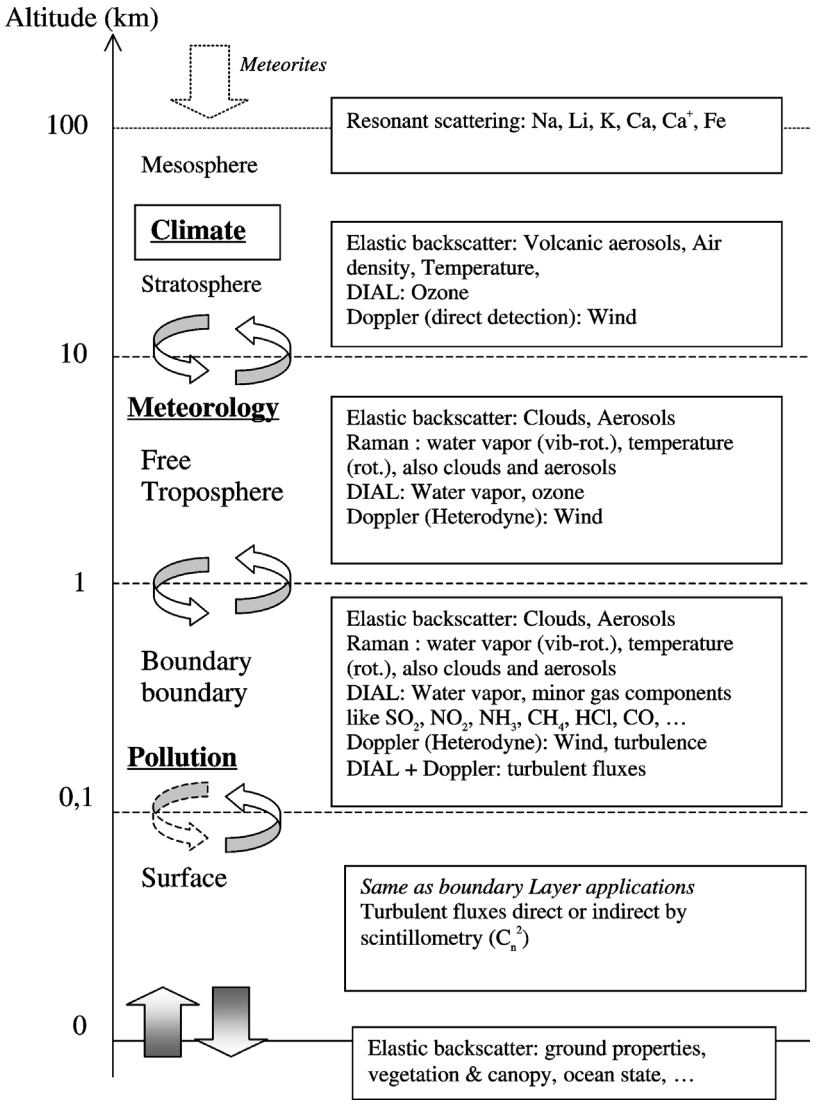

Fig. 1. Vertical structure of the atmosphere (log scale in km) and relevant Lidar applications. Double arrows indicate the interfaces and exchange regions between the main atmospheric reservoirs, and exchange processes with the surface.

ground to track satellite or Earth observation from space. Over the years, Lidar applications have spanned a broad range of applications in research and industry. The Lidar technique has been applied to (i) atmospheric sounding (see Fig. 1), (ii) terrain and city mapping, (iii) canopy and vegetation characterization, (iv) bathymetry, and (v) geologic features and the Earth's surface. The atmospheric community is more research oriented (see http://iclas.hamptonu.edu/) whereas a smaller user community committed towards operational applications and servicing deals with items 2, 3 and 4 (www.airborne1.com). Several books have been published on Lidar and especially on atmospheric Lidar [1], so the objective of the paper is to review the Lidar technique and the progress accomplished in the past forty years, to outline the link between spectroscopy and remote sensing, and finally to present the contribution of the French community.

Lidar started in the 1930s well before the discovery of the laser in 1960. It is noticeable that successful pioneering works on pulsed-light cloud-height detectors were developed in France as early as 1935 [2], and it is unfortunate that this research was stopped during World War II. The technique received operational application in the United States some years later. Along the same line, in the 1950s, successful studies were conducted with powerful searchlights on the upper atmosphere [3]. All these works paved the way for Lidar using laser, showing that active optical remote sensing technique has a great potential, provided a coherent light transmitter, as in radar, is available for the applications. Actually, the applications of Lidar systems to the remote sensing of atmospheric properties and composition were appreciated soon after the discovery of the laser. The decisive step was

the availability of the giant pulse (Q-switch) ruby laser. Soon after, laser emission in various active materials, i.e., solid, liquid, gaseous, and tunable lasers (especially dye lasers at the time), combined with non-linear optic techniques (harmonic generation, optical parametric oscillator, stimulated Raman shifter) enable the coverage of the entire optical spectrum from ultraviolet to infrared.

The name Lidar was cast in the 1950s [4] in analogy with radar using the word 'light'. Other names like Ladar (using Laser instead of light) or Laser radar are still in use but less frequently. However, because Lidar and Radar techniques rely on the same principles for scattering, propagation and detection of electromagnetic waves, the analogy helps meaningful concept transfer between the two techniques. The enhanced performance and greater flexibility of Lidar compared with optical probing techniques using non-laser energy sources, and its ability to extend meteorological radar techniques to the detection of very small particles, made possible new concepts of remote observation of the atmosphere. The first Lidar measurements of the upper atmosphere using a Laser transmitter were made in 1963 [5]. Then, in less than a decade, the basic atmospheric Lidar techniques: elastic scattering, Raman scattering, differential absorption and Doppler have been successfully demonstrated. However, the technology was well behind the expectation of the Lidar researchers to match the need for practical applications. Looking back to the Lidar venture, it is quite clear that much of progress was driven by new technologies coming from outside the scientific community. Computers and digital electronics that have improved tremendously during the last decades are two striking examples. Earlier Lidar studies used a dual-beam oscilloscope and Polaroid paper to record the signals on the flight. Lasers also improved in the meantime. Low pulse repetition frequency Ruby laser (1 or 2 shots per minute) in the early times are substituted today by reliable high performance Nd^{3+}:YAG laser available off-the-shelf including efficient frequency conversion. Some forty years ago, the researchers used to build their own laser prior to getting into Lidar applications. The same skills were needed for recording, processing and storing the data using oscilloscope devices and early computers.

The article presents the basic atmospheric Lidar in Section 2. Section 3 presents Lidar systems. Section 4 addresses the various techniques. Section 5 outlines the importance of spectroscopy in Lidar. Sections 6 and 7 presents the activities conducted in France, Section 6 addressing upper- and middle-atmosphere, while Section 7 addresses lower atmosphere applications.

2. Basic atmospheric Lidar

Remote sensing by Lidar involved three steps (see Fig. 2):

(1) a laser pulse is transmitted into the atmosphere to profile structural characteristics and composition;
(2) the light pulse interacts with individual scatterers, i.e., air molecules, particles or atoms, these targets may absorb, and they scatter the laser light in all direction resulting in an attenuation of the laser beam;
(3) the light scattered in the backward direction to the Lidar system is collected by a receiver telescope, then it is detected and processed to provide the Lidar signal.

Optical filtering is usually required before detection to improve the signal-to-noise ratio for better performance in range and sensitivity. Further processing of Lidar signals enable to retrieve atmospheric profiles along the line-of-sight. Most Lidar systems are set in a monostatic arrangement where the transmitter and receiver are at the same location. Fig. 2 is an example of coaxial set up (transmitter and receiver axes are identical). Some applications at long range make use of paraxial configuration to limit the useful signal dynamics below few hundreds. In any case, there exists a blind zone at short range, as displayed on Fig. 2, that depends on Lidar configuration and transmitter/receiver characteristics.

As displayed on Fig. 2, a pulsed laser emission enables range resolved measurements along the Lidar line-of-sight as the probing pulse travels in the medium. The range to the moving scattering volume is $r = ct/2$ for a Lidar signal detected at time t (the probing pulse is sent out at $t = 0$), c is the speed of light. It turns out that 1 µs corresponds to 150 m. The scattering volume is materialized by half the laser pulse duration $\Delta r = ct_\ell/2$ that also results in range ambiguity. In Lidar, range resolution is dictated by various factors, i.e., the pulse duration (t_ℓ), the detection response time and duration of processing range gate. In the atmosphere, individual scatterers are in motion (Brownian motion, turbulence, advection) and have random phase position. Their contributions to the Lidar signal are independent and result from an addition of scattered amplitudes. The optical power collected at time t is

$$P(t) = \left[\sum_i a_i \exp\left[j\omega(t - 2r_\varsigma/c)\right]\right]^2 \tag{1}$$

where a_i is the scattered light field amplitude, ω is the scattered frequency assuming a monochromatic laser emission, $t = (2r_\varsigma/c) - \varsigma$, with $0 \leqslant \varsigma \leqslant t_\ell$, r_ς is the scatterer position (r is an average of r_ς). After some calculation, it becomes [6]

$$P(t) = \sum_i a_i^2 + 2\sum_{i<k} a_i a_k \cos\left[(\omega_i - \omega_k)t + (\varphi_i - \varphi_k)\right] \tag{2}$$

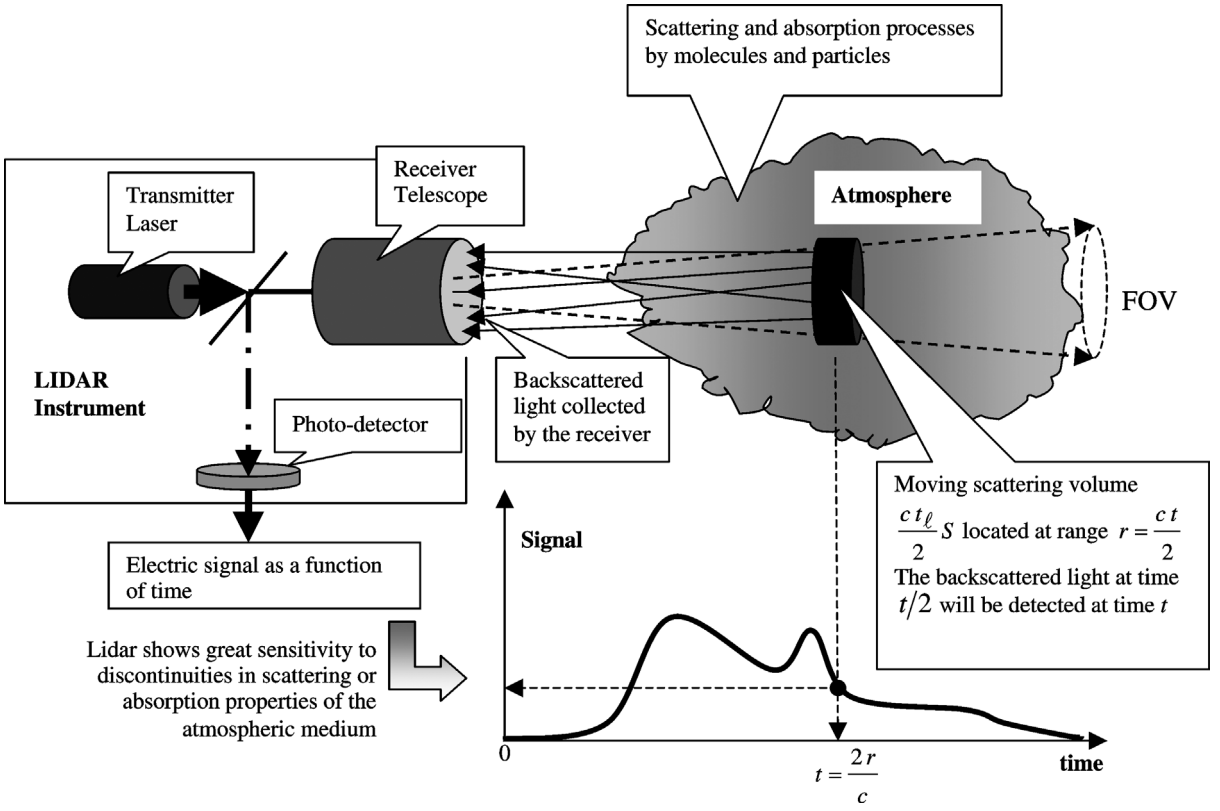

Fig. 2. Schematic of remote sensing by Lidar involving three steps: (1) a laser pulse is transmitted into the atmosphere to profile the structural characteristics and composition, (2) the light pulse interacts with individual scatterers, i.e., air molecules, particles or atoms, that results in scattering and attenuation of the laser beam, (3) the light scattered in the backward direction to the Lidar system is collected by a receiver telescope, then it is detected and processed to provide useful Lidar signal. The laser beam divergence is smaller than the receiver field-of-view $FOV \approx 1.3(A/r^2)$, A is the telescope area.

The first term is the sum of the intensities of each scatterer, while the second term is the sum of cross terms that bear the signature of scatter motion and phase position. In direct detection as displayed in Fig. 2, only the first term (dc component) is meaningful. In heterodyne detection when the laser beam of a cw local oscillator is superimposed on the photomixer detector, the second term (ac component) is detected as a radio frequency (rf) current with a carrier frequency equal to the off set frequency between the transmitter laser and the local oscillator plus a Doppler frequency shift. The rf signal enables us to measure directly the velocity of the scatterers.

The Lidar (budget) equation links the collected power as a function of range or time to atmospheric and instrument variables

$$P(r) = K_{\mathrm{op}}\beta(r)r^{-2}T_1(r)T_2(r) \tag{3a}$$

$$T_i(r) = \exp\left(-\sum_j \int_0^r \mathrm{d}x\,\left(\alpha_{\mathrm{sca},\,j}(x) + \alpha_{\mathrm{abs},\,j}(x)\right)\right) \tag{3b}$$

$K_{\mathrm{op}} = (c/2)EAm$ is an instrumental constant that accounts for the laser energy (E), collecting aperture (A) and optical component efficiency (m). Eq. (3a) applies also after detection and digitization using a constant that accounts for photo detector quantum yield $(q \leqslant 1)$. In (3a) the range is substituted to time $(r = ct/2)$. In direct detection the optical power is $P(r) = \sum_i a_i^2$ (see (2)). In the visible domain, a relative calibration on the molecular signal eliminates K_{op} from (3a). Eq. (3a) is an approximation for short probing pulse and short detection response time, otherwise it is a double convolution product. The set of Eqs. (3a) and (3b) are the foundation of Lidar techniques presented in Section 4.

The volume backscattering coefficient $\beta(r)$ in $m^{-1}sr^{-1}$ holds for all scatterers in the volume sets by the range ambiguity and beam diameter. Subscripts m and p stand for molecules and particles, respectively, $\beta(r) = \beta_m(r) + \sum_j \beta_{p,\,j}(r)$, $T_i(r)$ is the one-way transmission to and from the target. Two transmissions are considered for non-elastic vibrational Raman scattering

that results in large frequency shift. Otherwise it is simply $[T(r)]^2$. The one-way transmission depends on extinction coefficients by scattering $\alpha_{\mathrm{sca},j}(r)$ and absorption coefficients $\alpha_{\mathrm{abs},j}(r)$, subscript j stands for particles and molecules in the light path. Multiple scattering processes in dense media (i.e., water clouds) and diffraction effects in large (crystal) particles break the single scattering approximation that is used to derive (3a) and (3b). These multiple scattering processes may be accounted for using an empirical parameter η $(0 \leqslant \eta \leqslant 1)$ in transmission, i.e., $\eta\alpha_{\mathrm{scat},p}$. Multiple scattering are usually treated as unwanted processes. However, some new research uses them to derive relevant information from clouds [7]. In off-beam axis Lidar multiple scattering enables to derive dense cloud macroscopic properties, i.e., optical depth and geometrical thickness [8].

The efficiency of light-matter interaction $\beta(r)$ is a key that dictates the overall instrumental budget (see (3a)). The volume backscattering coefficient depends upon the wavelength, and the number, size and dielectric properties of the scatterers. Much of the particulate matter in suspension in the atmosphere is of the same order of size as optical wavelengths (0.3 to 10 μm). This leads to resonant effects and the magnitude of backscattering from each particle depends on a complicated manner upon the size/wavelength ratio $x = 2\pi r'/\lambda$, where r' is the particle equivalent radius. In this so-called 'Mie scattering regime', the variations in backscatter from an assembly of variously sized particles tend to average out and a smooth dependency with x is expected. Independent contribution of particles results in $\beta_p \approx \sum_i n_i \pi (r_i')^2$ that varies directly with the summation of the geometrical cross-sections without a strong dependence upon wavelength, n_i is the particle number density. Scattering by molecules (or nanometer particles) follows a different pattern in the so-called 'Rayleigh scattering regime' such $\beta_m \approx n(r')^6\lambda^{-4}$. Non-elastic Raman scattering processes by molecules involving vibrational-rotational or rotational states follows the same dependency but the volume backscatter coefficients are some 3 orders of magnitude smaller. The volume backscattering coefficient also has dependence upon polarization. The energy backscattered will have polarization characteristics that will depend upon the nature of the scatterers. In general terms, the controlling factor is the shape and orientation of the particles. No depolarization occurs for single scattering from microscopic spherical particles, depolarization factor is only 1.4% for air molecules probed with linearly polarized laser emission, it can reach up to 100% for ice crystals in cirrus clouds. Resonant scattering by atoms results in very large scattering cross section many orders of magnitude larger than the values experienced by elastic scattering, i.e., Mie and Rayleigh scattering regimes. Air dielectric gradients due to pressure, temperature, or humidity variations will also produce backscattering of electromagnetic energy like in radar, but in practice, this effect is quite negligible at optical wavelengths.

3. Lidar systems

The coaxial Lidar system in Fig. 2 displays the main components, i.e., a laser transmitter, a telescope receiver, a photo-detector associated to an electronic unit. It is essential to maximize the passive contributors to the Lidar budget in order to limit the demand on the laser that still remains the sensitive part of Lidar system. Today, a broad choice of commercial lasers is offered to the scientific community. Nd^{3+}:YAG laser combined with frequency converter (harmonic generation, optical parametric oscillator, stimulated Raman shifter) receives a great many applications in atmospheric Lidar because they are compact, reliable and easily affordable. Lasers using gaseous active medium, i.e., exciplex lasers in the UV (XeCl at 351 nm or XeF at 308 nm), and CO_2 laser in the 10 μm region, are also used for the applications, but at a lesser degree. New fiber lasers based on Yt3+ or Er3+ ion doping in solid matrix that operate in the near IR around 1.6 μm have a great potential for elastic backscatter and wind application as presented in Section 4. These lasers are currently developed for telecommunication applications. A beam expander may be useful to decrease the laser divergence, in order to reduce the receiver field-of-view (FOV) when stringent filtering of background light is required to achieve high signal-to-noise ratio. Optical photo detectors operating in the visible (PMT), near IR (avalanche photodiode) and thermal IR (photodiode) work quite satisfactory even if PMTs have limited quantum yield ($q \leqslant 0.15$), and photodiodes carry internal noise that limits the performance. Some progress are still expected in this area, and it is only recently that improved photo detector in the 2 μm domain could be made available in the next future. After detection, the electric signal is sampled by an analog digital converter (ADC) and stored on a computer. Today, high performance 20–50 MHz/10–12 bits ADCs and powerful computers are available off-the-shelf at a reasonable price. A high digitization rate is an important item because it enables meaningful calibration in UV to near IR on molecular signal. When the signal is too weak the detection unit is based on photon counting instead of electric current. Minimum detectable Lidar signal (in terms of variance) is determined by (i) detection noises due to Lidar signal and unwanted background solar light or infrared emission entering the receiver, or (ii) the sensitivity of the detection unit. The signal-to-noise ratio may be improved by a significant factor $\sqrt{N}$ by an averaging of N independent realizations. In some cases atmospheric correlation limits the improvement. Lidar measurements at medium- or long range are conducted in relatively high transmission region, i.e., atmospheric windows. The Lidar signal may vary by several orders of magnitude due to r^{-2} and $\beta(r)$ (see (3a)) whereas the linearity (within ± few percents) of the detection unit is limited to few hundred. Linearity is a key to ascertain changes in $P(r)$ to atmospheric backscatter or transmission. In practice, large signal dynamics is handled using beam splitter(s) and several detection units. In general, Lidars combine several channels at different wavelengths (355, 532 and 1064 nm for elastic scattering using Nd^{3+}:YAG Laser), two cross polarizations

at one wavelength (the laser transmitter is linearly polarized), and one (or more) Raman channel(s) for N_2 (or O_2 and H_2O) scattering for better retrieval of particle extinction coefficient and water vapor mixing ratio (see Section 4). Fixed line-of-sight measurements are frequently used for the application. However, scanning devices are used for wind application to provide with different perspectives to retrieve velocity vector or in pollution monitoring to sample an atmospheric volume.

Lidar measurements are conducted from the ground but also from other platforms like aircraft, ships, and satellite. The space odyssey started in the 1990s with LITE [9] and ALISSA [10] programs. Airborne Lidars in up- or down-looking configuration permit measurements over remote and regional areas difficult to access and not covered by ground based Lidar. Because they can fly faster than air mass movements, they give access to medium-scale patterns while space-based Lidar can give access to large-scale patterns. For down-looking visible systems, the inverse range squared decrease is somewhat compensated for by the increased backscattering due to increased atmospheric density. The key issue in airborne Lidars is the availability of research aircraft to the scientific community. Some disadvantages include the paucity of flight opportunities, the inherent cost for aircraft operation, and the increased system complexity due to space constraints, uneasy port access to fire the Lidar, power limitation and electro-magnetic interferences with the navigation system. However, despite these inconveniences, airborne Lidar programs have been conducted in the USA and in Europe to be later involved successfully in field campaigns addressing meso-scale meteorology and climate objectives. On the technology side, airborne Lidar is the link between ground-based and space-borne Lidars as demonstrated by the activities conducted at NASA in the USA and CNES in France.

4. Lidar techniques

Four range-resolved Lidar techniques based on pulsed Lidar are currently used in atmospheric sciences. They are based on (1) elastic scattering by particles and molecules, (2) non-elastic Raman scattering by molecules, (3) differential absorption by minor gaseous species such as H_2O, O_3, CO_2, (4) Doppler frequency shift associated to the motion of particles and molecules. All these techniques can be discussed with the help of (3a) and (3b). In most cases, quantitative Lidar analysis requires careful instrument calibration. The direct problem consists of expressing the Lidar signal as a function of atmospheric and system variables. The inverse problem consists in the retrieval of atmospheric variables from the Lidar signal using appropriate estimator and additional information. The estimator performance is evaluated in terms of statistical error and bias, and compared to the statistical limit set by the Cramer–Rao lower bound or maximum likelihood. This aspect of Lidar processing had made tremendous progress in the last decade in association with expanding computer capability.

4.1. Elastic scattering Lidar

The elastic scattering Lidar technique is the simplest, and can be made even simpler if operated at one single wavelength (one channel). It is widely used for atmospheric applications in the boundary layer dynamics to temperature measurement in the middle atmosphere. Assuming no absorption processes, (3a) and (3b) result in an equation with one constant K and two unknowns: total backscatter and total extinction

$$P(r) = Kr^{-2}\big(\beta_p(r) + \beta_m(r)\big)\exp\left(-2\int_0^r \mathrm{d}x\,\big(\alpha_{\mathrm{sca},p}(x) + \alpha_{\mathrm{sca},m}(x)\big)\right) \tag{4}$$

To retrieve $\beta_p(r)$ or $\alpha_{\mathrm{sca},p}(r)$, a second equation is needed. From general considerations on scattering it written as $\beta_p(r) \cong k_p\alpha_p(r)$ where k_p is independent of range. This is an approximation for limited range. However, k_p does not depend strictly on range if the size distribution and composition are constant, only the total density number of particles is allowed to vary. For molecules it is equal to $k_m = 3/8\pi$. Molecular contributions $\beta_m(r)$ and $\alpha_{\mathrm{sca},m}(r)$ are calculated using temperature profile and surface pressure information provided by nearby radiosonde or meteorological model and so eliminated from (4). The instrumental constant K is determined by relative calibration on molecular signal assuming a clean zone free of particles at some range, or hard target calibration. The first technique is applicable from UV to near IR and it results in an accuracy of few tens of percents. Target calibration is not an easy task and results in lower accuracy (about a factor 2). But it is the only possibility in the IR domain.

Several techniques have been proposed to solve the set of two equations, i.e., (4) and $\beta_p(r) \cong k_p\alpha_p(r)$. They are based on (i) integral equation to retrieve the particulate optical depth or volume extinction (or backscatter) coefficient, (ii) Bernoulli differential equation for volume extinction (or backscatter) coefficient, or (iii) iterative solution. Details and references are provided in Ref. [1]. Identical solutions are derived for integral or Bernoulli differential equation solutions. Both retrieval techniques provide forward (from closer to farthest range) and backward solutions (farthest to closer range). The backward technique is numerically more stable but the reference value is harder to define. As an example, Fig. 3 displays time series of volume backscatter coefficient at 532 nm (upper panel), depolarization ratio at 532 nm (middle panel), and apparent Angstrom

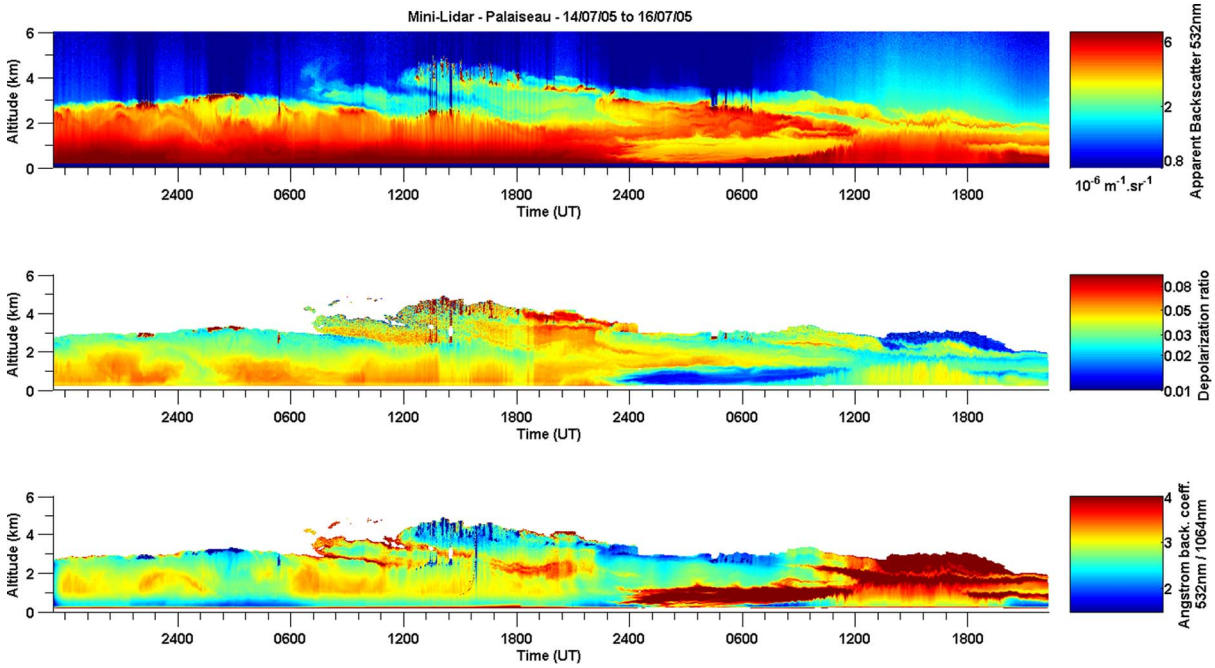

Fig. 3. Vertical profiling by an elastic scattering mini-Lidar operated at the Laboratoire de Météorologie Dynamique in Palaiseau. The time series span over 56 hours continuously. After processing the 3 panels displays Lidar information as a function of altitude, upper panel: apparent volume backscatter coefficient (not corrected for transmission) at 532 nm, middle panel: depolarization ratio at 532 nm, lower panel: apparent Angstrom coefficient derived from color ratio. Each measurement is an average of 10 seconds (200 shots). The relative calibration at 532 and 1064 nm (scattering and depolarization) are made using molecular signal at clean altitude range (free of particle).

coefficient derived from color ratio (lower panel) as a function of altitude. These measurements were performed by a mini-Lidar operated by Laboratoire de Météorologie Dynamique in Palaiseau. The time series span over 56 hours continuously. A vertical profile is recorded in 10 seconds (averaging 200 Lidar measurements). Calibrations at 532 and 1064 nm make use of molecular signals. The ratio of calibrated signals at 532 and 1064 nm is the so-called color ratio. The effective Angstrom coefficient is the logarithm of the color ratio. In the boundary layer between the surface and about 2 km, it varies from 4 (as expected for molecules) to about 1.5 for aerosol particles.

4.2. Raman Lidar

The scattering of light by molecules involves elastic (see Section 4.1) and inelastic spontaneous Raman processes, simultaneously. The Raman Lidar technique makes use of the weak inelastic scattering by diatomic (N_2, O_2) or three atom molecules (H_2O, O_3). Raman scattering results in a frequency shift to longer (Stokes) or shorter (anti-Stokes) wavelengths. The amount of frequency shift corresponds to vibrational-rotational or rotational energy that is characteristic of a molecule (spectroscopic information). The receiver narrow band filter needs to be tuned to the Raman shifted wavelength, i.e., 408 nm for water vapor and 387 nm for nitrogen when the laser wavelength is 355 nm. Also, stringent rejection of elastic scattering is required (several orders of magnitude). Few molecules are suitable for Raman Lidar application due to their limited abundance in the atmosphere. In practice, water vapor (wv) concentration involved nitrogen (nit) or oxygen as reference gases. Using (3) for H_2O and N_2, and taking the ratio it comes

$$\frac{P_{\mathrm{wv}}(r)}{P_{\mathrm{nit}}(r)} = \frac{K_1}{K_2}\frac{\beta_{\mathrm{wv}}(r)}{\beta_{\mathrm{nit}}(r)} = \frac{K_1}{K_2}\frac{\frac{\mathrm{d}\sigma}{\mathrm{d}\varpi}\big|_{\mathrm{wv}}}{\frac{\mathrm{d}\sigma}{\mathrm{d}\varpi}\big|_{\mathrm{nit}}}\frac{n_{\mathrm{wv}}(r)}{n_{\mathrm{nit}}(r)} \tag{5}$$

The Raman scattering cross-sections $(\partial\sigma/\partial\varpi)$ are inputs from spectroscopic databases. The system constant for the two channels may be different and need a careful calibration. Also, (5) assumes the same atmospheric transmission at the two wavelengths. Solving (5) for water-vapor mixing ratio $\rho_{\mathrm{wv}}(r) = n_{\mathrm{wv}}(r)/n_{\mathrm{air}}(r)$ gives

$$\rho_{\mathrm{wv}}(r) = K\frac{P_{\mathrm{wv}}(r)}{P_{\mathrm{nit}}(r)} \tag{6}$$

Most often, Lidar measurements are calibrated frequently against in situ observations using radiosonde. Other techniques that use diffuse daylight to determine the transmission ratio of the two channels enables to calculate K. The calibration error remains of the order of 5% [11]. Raman measurements do not require specific laser wavelengths contrary to the differential-absorption Lidar technique (see Section 4.3). Because of the λ^{-4} dependence UV emission wavelength are to be preferred ($\lambda \geqslant 320$ nm). However, the solar-blind region has also been used to avoid daylight background [12]. The Raman Lidar technique is used for

(i) density measurement of gaseous components based on vibration-rotation scattering, i.e., water vapor and ozone,
(ii) temperature measurement based on rotational scattering and
(iii) particulate extinction in order to separate the backscatter and extinction contributions that are inextricably linked in elastic backscatter Lidar.

Eq. (4) for vibrational–rotational Raman scattering on N_2 molecules results in a simpler equation involving $\alpha_{\mathrm{sca},p}$ but not β_p. More recently Raman Lidar received a new application to measure liquid water content. Wavelengths between 320 and 550 nm are best suited for this application. This spectral domain is typically in the range capability of Nd^{3+}:YAG laser (355 and 532 nm). The error of Raman Lidar measurements is dominated by statistical detection noise; systematic error (bias) mainly arises from the calibration procedure.

Atmospheric temperature profiling in the lower atmosphere considers pure rotational Raman scattering. Two signals scattered by nitrogen molecules are selected in the anti-Stokes and Stokes spectra located on each side of elastic (Rayleigh) line. However, because the populations in the anti-Stokes quantum states are very sensitive to temperature, it is preferable to select the two signals in the anti-Stokes spectrum using narrow band filters at 529.1 and 530 nm for a laser emission at 532.1 nm [13].

4.3. Differential Absorption Lidar (DIAL)

Differential-absorption Lidar or DIAL technique considers two wavelengths transmitted one after the other in the atmosphere. For narrow line absorption spectra like water vapor, one line, so-called λ_{on}, is usually set at line center to correspond to a significant optical depth ($\cong 1$) while the other line, λ_{off}, is used as reference with negligible absorption. For broadband absorption spectra like ozone, the spectral difference corresponds to an optical depth $\cong 1$. This magic number comes from a detailed error analysis using analytical or numerical solutions [14,15]. It is easily understood if one considers that the two signals will be not so different at low optical depth and the on-signal will be negligible if the optical depth is too large. The optimum in optical depth is broad around unity. Using (3) for on- and off-wavelengths results in

$$\frac{P_{\mathrm{on}}(r)}{P_{\mathrm{off}}(r)} = \frac{K_{\mathrm{on}}}{K_{\mathrm{off}}} \exp\left(-2 \int_0^r \alpha_{\mathrm{on}}(x)\,\mathrm{d}x \right) \tag{7}$$

Assuming that the two constants are equal, and the non specific transmissions (scattering by molecules and particles) are also equal, and substituting the difference in absorption cross-section ($\Delta\sigma_{\mathrm{abs}}$) and specie number density for α_{on} it results in

$$n = \frac{1}{2\Delta\sigma_{\mathrm{abs}}} \frac{\partial}{\partial r} \left(\mathrm{Ln}\left(\frac{P_{\mathrm{off}}(r)}{P_{\mathrm{on}}(r)} \right) \right) \tag{8}$$

In practice some averaging over a range gate (Δr) is required to improve the signal-to-noise ratio

$$n = \frac{1}{2\Delta\sigma_{\mathrm{abs}}\Delta r} \left(\mathrm{Ln}\left(\frac{P_{\mathrm{off}}(r+\Delta r)}{P_{\mathrm{on}}(r+\Delta r)} \frac{P_{\mathrm{on}}(r)}{P_{\mathrm{off}}(r)} \right) \right) \tag{9}$$

In practice, some regularization of the Lidar signals is needed before taking the logarithm of the ratio.

One main drawback in the DIAL technique is the possible interferences with species that absorb in the same spectral region, i.e., SO_2 for O_3 in the UV or water vapor for CO_2 in the 2 μm spectral region. Other limitations come from inaccurate spectroscopic data, inaccurate spectral positioning, and transmitter spectral purity. So, the choice of the absorption line pair needs a great deal of attention. The range-resolved DIAL technique has been demonstrated for water vapor some 40 years ago using a temperature tuned Ruby laser [16]. The main strengths of DIAL in a ground-based application for water vapor profiling, as an example, are its independence from external calibration, excellent daytime performance for high range resolution studies in the boundary layer and high accuracy routine observations in the mid troposphere. Any Lidar is dependent on the availability of suitable laser sources, but for DIAL, the requirements are especially inflexible because the required characteristics are determined by the spectral features of the molecules to be studied. Vertical profiling of stratospheric ozone has been reported from the ground in the 1970s [17] at the time the ozone depletion scenario was poorly documented. Since then, the Lidar technique has improved and a 'Network for the detection of the Stratospheric Changes (NSDC)' has established ozone climatology for more than a decade.

4.4. Doppler Lidar

The Doppler Lidar technique for wind velocity measurement is based on the frequency shift due to the so-called Doppler effect. Atmospheric Lidar application at optical wavelength makes use of scattering by air molecules and microscopic particles moving with the wind. The frequency shift is

$$\Delta\nu|_{\mathrm{Dop}} = -2\frac{V_r}{\lambda} \tag{10}$$

A factor 2 accounts for two successive shifts between laser and scatterers and then between scatterers and receiver, V_r is the radial velocity of the scatterers along the Lidar line-of-sight. A 1 $\mathrm{m\,s^{-1}}$ accuracy requires a relative laser frequency stability $2V_r/c \cong 10^{-8}$ that is demanding even for an injection-seeded transmitter. Doppler frequency shift measurements do not require specific laser wavelengths. A retrieval of the wind vector needs at least two different perspectives. Conical scan (velocity azimuth display) or raster scan as in the radar technique are used also to sample the atmosphere.

Basically, two range-resolved Doppler Lidar techniques are currently used depending on the nature of the scatterers:

(i) direct detection using molecules for stratospheric application, a dual-Fabry–Perot interferometer is used as receiver to sample the broad spectrum ($\Delta V_r \cong 300$ $\mathrm{m\,s^{-1}}$) scattered by air molecules [18];
(ii) heterodyne detection when the aerosols loading is sufficient [19].

Direct detection estimator is based on the ratio of two signals issued from a dual Fabry–Perot interferometer. Heterodyne detection makes use of the narrow spectral signal ($\cong 1$ $\mathrm{m\,s^{-1}}$) from aerosol particles and frequency estimators as in radar. Numerous publications have addressed signal processing and frequency estimator in the last two decades. Today, the best frequency estimators have a performance within a factor 2 with respect to the Cramer–Rao lower bound or Maximum likelihood estimator. A comparison of direct and heterodyne Doppler techniques shows that ultimate accuracy is dictated by the same statistical limit $\delta V_r \cong (\Delta V_r/\sqrt{N_e})$ where ΔV_r is the half width at half maximum of the scattered light, $N_e = q\gamma P(r)/h\nu$ is the number of photoelectrons for a measurement, where $\gamma \leqslant 0.4$ is the heterodyne efficiency (it is equal to unity in direct detection) that accounts for partial degree of coherence of atmospheric signals. Heterodyne detection results in speckle effect with large rf signal fluctuations on a shot-to-shot basis. Frequency estimates in heterodyne Lidar are conducted on a shot-to-shot basis, then they are improved by further averaging as square root of the number of independent realizations. In direct detection, averaging is conducted on N_e.

In practice, the required frequency stability (10^{-8}) cannot be achieved, so, in heterodyne detection, Doppler frequency shift is the difference between frequency estimates on atmospheric signal ($\Delta\nu_D + \Delta\nu_{\mathrm{off}}$) and on reference signal, i.e., beat note between laser transmitter and local oscillator ($\Delta\nu_{\mathrm{off}}$). Ground based and airborne heterodyne Doppler Lidars have been operated in the 10 and 2 μm spectral region using CO_2 laser and solid-state laser, respectively. Direct detection Lidar are operated in the visible (532 nm) and UV (355 nm). Both techniques have advantages and some drawbacks: heterodyne detection needs a sufficient aerosol loading in order to deal with sufficient signal-to-noise ratio, even if frequency estimator are still efficient at low $SNR \geqslant 0.1$ whereas direct detection requires much larger $SNR \geqslant 10$. Direct detection operates better in clear air for a low scattering ratio still needs correction even if the Lidar has been designed to be less sensitive to aerosols scattering. Nevertheless, both techniques have been successfully used from ground [20] and airborne platforms [21]. The Wind Lidar system that is developed by the European Space Agency to be the heart of the Atmospheric Dynamic Mission is based on direct detection at 355 nm using a powerful Nd^{3+}-YAG laser and 1.5-m diameter telescope (see http://www.esa.int/export/esaLP/ESAES62VMOC_aeolus_0.html).

5. Atmospheric spectroscopy

Spectroscopy plays a key role in Lidar for it is involved in the light-matter interaction processes that govern the strength of the Lidar signal (see (3a), (3b)). Elastic molecular scattering $\beta_m(r)$ and $\alpha_{\mathrm{sca},m}(r)$ for air molecules have been measured in the laboratory with great accuracy. The so-called Rayleigh scattering has been discussed in depth [22] to define the various contributions as a function of pressure. However, even today, the various Lidar techniques are suffering from missing key spectroscopic information, inaccuracy or inexactness. As an example, the Brillouin doublet scattered by air molecules at atmospheric pressure is not known with sufficient accuracy, there exist no experimental data and the best model [23] does not treat gas mixtures. In Raman Lidar, the Raman cross sections $\partial\sigma/\partial\varpi$ (see (5)) are inputs taken from spectroscopic databases, and some inaccuracy requires a careful calibration. Any inaccuracy on absorption cross-section results in a bias on specie number density in DIAL technique (see (9)). The spectroscopic information dictates also the choice of the line pair to avoid interferences with species that absorb in the same spectral region. Some information like pressure shift of line center is lacking

for lines that could be potentially used for CO_2 DIAL measurements, as an example. In the past, the lack of relevant information on H_2O and O_2 molecules led Lidar researchers to conduct their own experiment using a multi-pass cell [24–28] or the photo-acoustic technique [29,30]. Relevant information have been obtained using other techniques like Intra-cavity absorption with pulsed or cw laser, Cavity ring down (pulsed laser), and High resolution Fourier-transform spectroscopy. More generally, many groups are actively involved in computational and experimental activities to improve the current HITRAN [31] (see also 'Cfa-ftp.Harvard.edu/pub/HITRAN-96') and GEISA databases [32]. Beside the research dedicated to molecules, particle spectroscopy is very active to determine key parameters β_p, $\alpha_{\mathrm{sca},p}$ and k_p especially for large particles like ice crystals [33] for the current spherical assumption used for years definitely has shown very limited applicability in practice. Various techniques are used including ray-tracing and Monte Carlo computation [34].

6. Activities in France: upper- and mid-atmosphere

The Lidar activity in France started at Service d'Aéronomie in the late 1960s initiated by Prof. J.E. Blamont, G. Mégie and M.-L. Chanin. The research activity was dedicated to the origin of metallic species, i.e., sodium atoms, around 100 km, using the resonant scattering Lidar technique [35] and later to middle atmosphere photochemistry with an emphasis on stratospheric ozone [36]. The measurements were conducted at the Haute Provence Observatory for good atmospheric transmission conditions (for such long range monitoring) and clear nights (low background light for improved signal-to-noise ratio). In the early days, the researchers developed their own tunable dye lasers. Fortunately, the best dye laser (using rhodamine 6 G) operates in the spectral domain that matches the sodium doublet at 588.9 nm. Dye molecules in a liquid medium offer the possibility to condensate all the laser energy in a tunable narrow line emission (about 1 GHz) provided a Fabry–Perot etalon is set in the resonator [37] or a diffraction grating sets at one end on the resonator. For an ultra narrow line emission several etalons or a combination of etalon and diffraction grating is required but the tunability was limited and erratic. The scattering cross section of resonant scattering cross section is so large that few atoms per cm^3 were detected after significant time averaging. Temperature measurements using the ratio of the sodium doublet component [38] is still in use today. Then, the search was directed to other metallic species like potassium at 766.4 nm [39], lithium at 670.8 nm [40], calcium at 422.7 nm and ionized calcium at 393.4 nm [41]. As a necessary step prior to any atmospheric measurements, the researchers developed new Nd^{3+}:YAG pumped dye lasers [42].

Stratospheric ozone was another key issue in atmospheric science in the early 1970s. The DIAL technique with systems operating in the ultra violet (Harley–Huggins bands of ozone between 280 and 320 nm) was suited to conduct the measurements from the ground using powerful dye laser and frequency conversion. Tunable frequency-doubled dye laser pumped by Nd^{3+}-YAG laser or fixed emission exciplex laser have been used for O_3 measurement. The first ground-based DIAL system based on dye lasers has been operational at OHP in 1977 [17,43,44]. Since then, the French community contributes to the Network for the detection of stratospheric changes (NSDC) involving three stations located at the Haute-Provence Observatory (Alpine station), Dumont d'Urville in Antarctica and La Réunion in the tropics. These Lidar stations are equipped in various Lidars and supplementary radiometers.

7. Activities in France: lower atmosphere

The successes obtained on tropospheric [45] and stratospheric ozone monitoring from the ground (see Section 6) led to DIAL application to other species such as SO_2 [45] and water vapor [46]. In the mid 1980s a new momentum was given to Lidar activities in France with the advent of a research aircraft Fokker 27 that could carry airborne Lidars. Service d'Aéronomie and Laboratoire de Météorologie Dynamique proposed to develop the meteorological airborne Lidar program LEANDRE in 3 steps, with the technical support of Technical Division of INSU/CNRS and Météo-France/CNRM. The program started with an elastic backscatter Lidar, LEANDRE-1, then a water vapor DIAL, LEANDRE-2, and finally a heterodyne Doppler Lidar, so-called WIND, after a Franco German cooperative program had been effective in the early 1990s. The airborne program was fully funded by CNRS and CNES in France. WIND has been funded by DLR in Germany. LEANDRE-1 was operational in 1990 and made a significant contribution to the international field campaign PYREX the same year [47] and later in numerous other programs. The DIAL Lidar that uses an on- and off-wavelength transmitter required the development of a new Alexandrite laser transmitter prior any Lidar deployment. So, the French scientists involved in the program have developed a two-wavelength dual pulse laser transmitter [48]. The water vapor DIAL Lidar was operational in 1996 [49] and involved in ACE-2 international field campaign in 1997, and later in MAP in 1999 and IHOP in the USA in 2002. The WIND Lidar was operational on board the DLR Falcon 20 in 1999 [19] and involved successfully in the international MAP field campaign the same year [21]. The WIND Lidar is based on CO_2 laser technology and a special laser transmitter was developed on purpose by French industry for this program. The research activity led also to the development of a Transportable Wind Lidar that was deployed successfully in the Rhine

valley during the MAP experiment [50]. In parallel with the meteorological airborne Lidar program, the chemistry community developed an airborne ozone DIAL so-called ALTO [51] that was successfully deployed in international field campaigns.

8. Conclusions

In the early days, building Lidar was difficult and the technique developed a reputation as something of an arcane art. Even single-wavelength elastic backscatter systems were complex and extremely costly and they required highly trained operators and too many frequent adjustments that made impossible to achieve long time series. These problems were worse for DIAL, and even worst for heterodyne Doppler Lidar, and so, as promising as the theoretical expectations and demonstration were, the DIAL and Doppler systems saw very limited applications for sometimes. For broad acceptance, Lidar systems in general needed simpler operation, much better reliability, software to produce real time reduced data, eye safety, standard and standardized measurement techniques and retrieval methods, and, last but not least, lower costs. Lidar researchers have made tremendous progress in all of these areas.

The French community, Service d'Aéronomie and Laboratoire de Météorologie Dynamique, have been involved since the beginning and made significant contributions to Lidar sciences and technology for more than 30 years now. Over the years Centre National d'Études Spatiales (CNES) and CNRS were two key partners that made possible the Lidar venture with considerable international success that will continue with the CALIPSO program developed under NASA/CNES cooperation (see http://www-calipso.larc.nasa.gov/ and http://smsc.cnes.fr/CALIPSO/Fr/index.htm). Also, the French community contributes significantly to the space-borne program ADM-ÆOLUS under development at the European Space Agency (ESA) to be launched in 2008. For the near future, the Lidar community raises some expectation for future activities in direction of the Earth-CARE mission at ESA and possible CO_2 and Climate mission as proposed in response to the call for ideas for the next ESA Earth Explorer Core Missions.

References

[1] E.D. Hinkley (Ed.), Laser Monitoring of the Atmosphere, Springer-Verlag, Berlin, 1976;
C.G. Bachman, Laser Radar Systems and Techniques, Artech House, Norwood, MA, Boston, London, 1979;
R.M. Measures, Laser Remote Sensing, Krieger, Malabar, FA, 1984;
V.A. Bankh, V.L. Mironov, Lidar in a Turbulent Atmosphere, Artech House, Boston, London, 1987;
A.V. Jelalian, Laser Radar Systems, Artech House, Boston, 1992;
A.F. Bunkin, K.I. Voliak, Laser Remote Sensing of the Ocean, Wiley, New York, 2001;
V.A. Kovalev, W.E. Eichinger, Elastic Lidar, Wiley, New York, 2004;
C. Weitkamp (Ed.), Lidar, Springer-Verlag, Berlin, 2005.
[2] R. Barthélemy, C. R. 222 (1946) 150;
R. Bureau, C. R. 222 (1946) 292–301;
A. Perlat, M. Petit, Mesures en météorologie, Gauthiers–Villars, Paris, 1961.
[3] L. Eltermann, Appl. Opt. 5 (1964) 1769–1776.
[4] W.E.K. Middleton, A.F. Spilhaus, Meteorological Instruments, Univ. of Press, Toronto, 1953.
[5] G. Fiocco, L.O. Smullin, Nature 199 (1963) 1275–1276.
[6] P. Salamitou, A. Dabas, P.H. Flamant, Appl. Opt. 34 (1995) 499–506.
[7] L.R. Bissonnette, in: C. Weitkamp (Ed.), Lidar, Springer-Verlag, Berlin, 2005.
[8] R.F. Cahalan, M. McGill, J. Kolasinski, T. Varnai, K. Yetzer, J. Atmos. Ocean. Tech. 22 (2005) 605–627;
I. Polonsky, S.P. Love, A.B. Davis, J. Atmos. Ocean. Tech. 22 (2005) 628–648.
[9] D.M. Winker, R.H. Couch, M.P. McCormick, Proc. IEEE 84 (1996) 164.
[10] M.-L. Chanin, A. Hauchecorne, C. Malique, Earth Planet. Sci. 328 (1999) 359.
[11] V. Sherlock, A. Hauchecorne, J. Lenoble, Appl. Opt. 38 (1999) 5816.
[12] D. Renault, J.-C. Pourny, R. Capitini, Opt. Lett. 5 (1980) 233.
[13] M.-L. Chanin, A. Hauchecorne, D. Nedeljkovic, Proc. SPIE 1714 (1992) 242.
[14] R.L. Byer, M. Garbuny, Appl. Opt. 12 (1973) 1496.
[15] G. Mégie, R.T. Menzies, Appl. Opt. 19 (1980) 1173.
[16] R.M. Schotland, in: Proceedings of the Third Symposium on Remote Sensing of Environment, Univ. Michigan, Ann Arbor, 1964.
[17] G. Mégie, J.Y. Allain, M.-L. Chanin, J.E. Blamont, Nature 270 (1977) 329.
[18] M.-L. Chanin, A. Garnier, A. Hauchecorne, Geophys. Res. Lett. 16 (1989) 1273.
[19] Ch. Werner, P.H. Flamant, O. Reitebuch, F. Köpp, J. Streicher, S. Rahm, E. Nagel, M. Klier, H. Hermann, C. Loth, P. Delville, P. Drobinski, B. Romand, Ch. Boitel, D. Oh, M. Lopez, M. Meissonnier, D. Bruneau, A.M. Dabas, Opt. Engrg. 40 (2001) 115–125.
[20] A. Garnier, M.-L. Chanin, Appl. Phys. B 55 (1992) 55.
[21] O. Reitebuch, Ch. Werner, I. Leike, P. Delville, P.H. Flamant, A. Cress, D. Engelbart, J. Atmos. Ocean Tech. 18 (2001) 1331–1344.

[22] A.T. Young, Phys. Today (1982) 42–48;
A.T. Young, Appl. Opt. (1981) 533–535.
[23] G. Tenti, C.D. Boley, R.C. Desai, Can. J. Phys. (1974) 285–290.
[24] B. Grossmann, C. Cahen, J.-L. Lesne, J. Benard, G. Leboudec, Appl. Opt. 25 (1986) 4261–4267.
[25] T.D. Wilkerson, G. Schwemmer, B. Gentry, L.P. Giver, J. Quant. Spectrosc. Radiat. Transfer 22 (1979) 315–331.
[26] L.P. Giver, B. Gentry, G. Schwemmer, T.D. Wilkerson, J. Quant. Spectrosc. Radiat. Transfer 27 (1982) 423–436.
[27] C. Cahen, B. Grossmann, J.-L. Lesne, J. Benard, G. Leboudec, Appl. Opt. 25 (1986) 4268–4271.
[28] B. Grossmann, E.V. Browell, J. Mol. Spectrosc. 136 (1989) 264–294.
[29] J. Bösenberg, Appl. Opt. 24 (1985) 3531–3534.
[30] K.J. Ritter, T.D. Wilkerson, J. Mol. Spectrosc. 121 (1987) 1–19.
[31] L.S. Rothman, and collaborators, J. Quant. Spectrosc. Radiat. Transfer 60 (1998) 665–710.
[32] N. Jacquinet-Husson, and collaborators, J. Quant. Spectrosc. Radiat. Transfer 62 (1999) 205–254.
[33] M.I. Mishchenko, J.W. Hovenier, L.D. Travis, Light Scattering by Nonspherical Particles, Theory, Measurements and Applications, Academic Press, San Diego, CA, 2000.
[34] V. Nöel, G. Ledanois, H. Chepfer, P.H. Flamant, Appl. Opt. 40 (2001) 4365–4375.
[35] J.E. Blamont, M.-L. Chanin, G. Mégie, C. R. Acad. Sci. Paris 274 (1972) 93–96.
[36] G. Mégie, Laser measurements of atmospheric trace constituents, in: R. Measures (Ed.), Laser Remote Chemical Analysis, Wiley, New York, 1988.
[37] G. Mégie, O. De Witte, Rev. Phys. Appl. 6 (1971) 341–343.
[38] G. Mégie, J.E. Blamont, M.-L. Chanin, in: K. Rawer (Ed.), Methods of Measurements and Results of Lower Ionosphere Structure, Akademie-Verlag, Berlin, 1974, pp. 27–32.
[39] G. Mégie, F. Bos, J.E. Blamont, M.-L. Chanin, Planet. Space Sci. 26 (1978) 27–35.
[40] J.-P. Jégou, M.-L. Chanin, C. R. Acad. Sci. Paris Sér. B 290 (1980) 325–329.
[41] C. Granier, J.-P. Jégou, G. Mégie, in: Proc. 12th Intern. Laser Radar Conf., Aix-en-Provence, France, 1984, pp. 229–232.
[42] C. Loth, Y.H. Meyer, F. Bos, Opt. Comm. 16 (1976) 310–313;
F. Bos, Appl. Opt. 20 (1981) 1886–1890.
[43] J. Pelon, P.H. Flamant, M.-L. Chanin, G. Mégie, C. R. Acad. Sci. Paris, Sér. II 292 (1981) 319–324.
[44] J. Pelon, G. Mégie, J. Geophys. Res. 87 (C7) (1982) 4947.
[45] G. Ancellet, G. Mégie, J. Pelon, R. Capitini, D. Renault, Atmos. Environ. 21 (1987) 2215–2226.
[46] C. Cahen, J. Pelon, P.H. Flamant, G. Mégie, C.R. Acad. Sci. Paris, Sér. II 292 (1981) 19–32;
C. Cahen, G. Mégie, P.H. Flamant, J. Appl. Meteor. 21 (1982) 1506–1515.
[47] P. Bougeault, A. Jansa, J.L. Attié, I. Beau, B. Bénech, R. Benoit, P. Bessemoulin, J.L. Caccia, J. Campins, B. Carissimo, J. Champeaux, M. Crochet, A. Druilhet, P. Durand, A. Elkhalfi, P.H. Flamant, A. Genoves, M. Georgelin, K.P. Hoinka, V. Klaus, E. Koffi, V. Krotoni, C. Mazaudier, J. Pelon, M. Petitdidier, Y. Pointin, D. Puech, E. Richard, T. Sotomura, J. Stein, D. Tannhauser, Ann. Geophys. 11 (1993) 395–418.
[48] J. Pelon, G. Megie, C. Loth, P. Flamant, Opt. Commun. 59 (1986) 213–218;
D. Bruneau, H. Cazeneuve, C. Loth, J.M. Pelon, Appl. Opt. 33 (1991) 3930–3937.
[49] D. Bruneau, P. Quaglia, C. Flamant, J. Pelon, Appl. Opt. 40 (2001) 3462.
[50] P. Drobinski, A.M. Dabas, C. Haeberli, P.H. Flamant, Boundary Layer Meteorology 99 (2001) 277–296.
[51] G. Ancellet, F. Ravetta, Appl. Opt. 37 (1998) 5509–5520.